JOURNAL OF PROPULSION AND POWER
Vol. 17, No. 4, July–August 2001

# High-Pressure Bipropellant Microrocket Engine

A. P. London,* A. H. Epstein,† and J. L. Kerrebrock‡
*Massachusetts Institute of Technology, Cambridge, Massachusetts 02139*

**The development of high-aspect-ratio, high-precision micromachining in silicon or silicon carbide suggests the feasibility of microfabricated, high-chamber-pressure chemical rocket engines. With high-speed turbopumps and valves incorporated onto the rocket chip, a number of propulsion cycles are possible. Such an engine, approximately 20 × 15 × 3 mm in size, operating at a 125-atm chamber pressure, would produce about 15 N of thrust using 300-s $I_{sp}$ propellants at a thrust-to-weight ratio of 1000:1. The feasibility of these engines has been investigated, and a liquid-cooled, pressure-fed thrust chamber and nozzle have been successfully designed, fabricated, and operated at a 12.5-atm chamber pressure to further evaluate the concept.**

## I. Introduction

THIS paper introduces the concept of micromachined, bipropellant, high-pressure liquid propellant rocket engines. These are complete, millimeter- to centimeter-sized, liquid propulsion systems fabricated using semiconductor manufacturing technology and materials. They consist of a regeneratively cooled thrust chamber and nozzle, turbopumps, and control valves. Manufactured in planar arrays on wafers of materials such as silicon, they can be regarded as rocket engines on a chip. Such microfabricated devices are generally referred to as micro mechanical and electrical systems (MEMS), and heat engines so made are known as power MEMS. Herein we give the background of this work, present possible applications of such devices, discuss the engineering constraints and solutions at this length scale, briefly outline the manufacturing process, and describe the progress made to date, including test results.

## II. Background and Concept

In 1997, Epstein and Senturia[1] suggested that MEMS heat engines in the millimeter- to centimeter-size range, with power densities similar to those of more familiar full-size devices, could be realized using semiconductor-derived micromachining technology of materials such as silicon or silicon carbide. The economic advantage of micromachining technology is that devices of very high mechanical precision (micro meters) and geometric complexity are fabricated in parallel, many (tens, hundreds, thousands) to a wafer, so that the per unit manufacturing cost can be relatively small when in large-scale production (as is the case for microelectronics). The first power MEMS device reported under development is a centimeter-sized gas turbine engine on a chip, consisting of a centrifugal compressor, combustor, radial inflow turbine, and fuel control valves.[2]

The engineering requirements of a bipropellant liquid-fueled rocket engine are in many ways similar to those of a gas turbine: cooled structures of high-temperature materials, high-pressure combustion, high-speed turbomachinery, and controls. This suggested that micro-gas-turbine technology could be adapted to realize high-pressure, turbopump fed, centimeter-sized rocket engines in the 5–50 N thrust range with specific impulse $I_{sp}$ approaching that of large-scale engines with similar propellants. The complete rocket engine system (thrust chamber and nozzle, turbopumps, and control valves) would be fabricated in wafer form and occupy less than a cubic centimeter, yielding a quite high thrust-to-weight ratio, in the range of 1000:1, due to favorable geometric scaling combined with the high strength to weight of the materials.

The engineering constraints imposed by the manufacturing technology, the materials, and the mechanics of small-scale devices can differ considerably from those of their more familiar full-sized brethren. Therefore, the empirical understanding, the engineering tools, and the optimal design space familiar from our experience with large-size engines may not be entirely applicable. The microrocket engine concept was initially explored in several theses at the Massachusetts Institute of Technology. London[3] first discussed the utility of such devices. Al-Midani[4] performed a preliminary study of a microexpander cycle engine using LOX and ethanol propellants. Protz[5] expanded this work by examining other cycles suitable for storable propellants. Lopata[6] and Faust[7] performed experimental heat transfer studies of propellants in microchannels at heat flux levels and geometries similar to those expected in the cooling channels of microthrust chambers. Frechette[8] demonstrated 1.4-Mrpm operation of a 4-mm-diam MEMS turbine suitable for powering a micro fuel pump. Francis[9] explored various applications of such engines including orbital launch vehicles with gross liftoff weights as low as 15 kg.

There are many possible applications for such microrocket engines, some are direct replacements for existing propulsion systems whereas others are entirely new systems enabled by the high-pressure microrocket engine concept. In the former category is stationkeeping of large geosynchronous satellites for which thrust levels in the 5–50 N range are adequate. In this case, a pump-fed bipropellant microrocket engine system would have higher $I_{sp}$ than monopropellant systems and the pump feed would permit low-pressure tankage and feed systems and, therefore, lower overall weight, compared to current pressure-feed propellant systems. Obviously, several or many of the engines can be used in parallel to realize higher thrust levels. For example, 3–10 microrocket engines operating in parallel could replace current 100–500 N thrust apogee kick engine technology.

A new concept that could be enabled by microrocket engines is micro launch vehicles, launch vehicles massing from a few tens to several hundred kilograms at launch. Given that global positioning system and MEMS-based inertial instrumentation technology is sufficiently advanced to realize guidance systems massing only a few tens of grams, such vehicles could boast payloads ranging from several hundred to several thousand grams into low Earth orbit. This concept broadens the term low cost access to space from cost per payload mass to include cost per mission. It is suggested that total launch costs of a few tens of thousands of dollars are feasible (assuming vehicle costs similar to those of tactical missiles of equivalent size).

Presented as Paper 00-3164 at the AIAA/ASME/SAE/ASEE 36th Joint Propulsion Conference and Exhibit, Huntsville, AL, 16–19 July 2000; received 19 August 2000; revision received 19 January 2001; accepted for publication 5 February 2001. 

*Research Assistant, Gas Turbine Laboratory, 77 Massachusetts Avenue, Room 31-265; aplondon@alum.mit.edu.

†R. C. MacLaurin Professor, Gas Turbine Laboratory, 77 Massachusetts Avenue, Room 31-265; epstein@mit.edu. Fellow AIAA.

‡Professor, Gas Turbine Laboratory, 77 Massachusetts Avenue, Room 31-265. Honorary Fellow AIAA.

Independent of the application, this technology has the potential to change the small end of the rocket engine business because it can commoditize thrust. The economic advantage of micromachining technology is that the per unit manufacturing cost can be small when in large-scale production. It is not unreasonable to think of engines in production costing as little as a few tens of dollars each (about the same as microelectronic devices of similar process complexity) and, thus, about equal in cost per unit thrust to very large engines. Reliability would be achieved as it is in the semiconductor industry, by painstaking attention to detail and process control checked with statistical sampling. Thus, various thrust levels are realized by assembling different numbers of qualified standard parts together (as is the case for computer memory) rather than engineering new motors for new applications as is done for rocket engines today.

As the first step in realizing a micro-high-pressure, bipropellant rocket engine, we have designed, built, and tested a cooled thrust chamber and nozzle for such a device. The remainder of this paper details this work.

## III. Requirements, Constraints, and Design Space

A feasibility study and modeling effort were completed to evaluate the design space of microrocket engines and delineate how this differs from that of traditional large-scale liquid rocket engines. This work considered oxygen and ethanol propellants in an expander cycle. The total heat load is sufficiently high that both propellants must be used as coolants. This section details the results of this design space study.

### A. Engineering Requirements

The applications discussed earlier assume that performance, usually expressed in terms of $I_{sp}$, can be maintained at or near the level currently realized in large-scale rocket engines. This in turn implies a number of engineering requirements, primarily high chamber temperature and pressure. The most critical of these is the need for a high chamber temperature, which must be on the order of 3000 K to reach an $I_{sp}$ near 300 s for the propellants considered here. This is well above the 1600-K melting temperature of silicon, which means that effective cooling of the chamber and nozzle walls is needed.

High chamber temperature requires complete combustion of the propellants to ensure that the full chemical energy of the propellants is released and available for conversion into the kinetic energy of the exhaust flow. The small scale of these rocket engines implies a correspondingly smaller residence time (100 $\mu$s) relative to large-scale engines (which constrains feasibility at scales smaller than considered here). High chamber pressure is required to ensure that the propellant molecules have sufficient collisionality to prevent vibrational freezing of the exhaust flow. Calculations suggest that at a chamber pressure of 1 atm, the vibrational relaxation time is of the same order as the nozzle flow time (1 $\mu$s), implying that chamber pressures of at least 10–20 atm are needed. Chamber pressure also directly impacts thrust-to-weight ratio. Thrust-to-weight ratio is essentially proportional to chamber pressure.

Rocket engines at these small length scales have increased wall area per unit volume compared to conventional-size engines, so that wall friction and heat transfer are concomitantly larger. However, as long as the chamber and nozzle are regeneratively cooled, there is no first-order impact on the engine performance because the thermal energy lost to the walls in this manner is recycled into the combustion chamber with the propellants. The boundary-layer displacement thickness is relatively larger, however, which must be accounted for in the nozzle design.

### B. Physical Design Constraints

There are four physical constraints on the design of the rocket system that limit the temperatures and pressures that can be realized in a microrocket engine and, therefore, constrain the achievable performance. These constraints are as follows.

#### 1. *Heat Flux Limit*

The chamber wall temperature must remain below the softening point of silicon to avoid structural failure (the yield strength of Si drops by a factor of two between 950 and 1100 K). This sets an upper limit on the hot-side temperature of a cooled wall. On the cold side, the wall temperature cannot be lower than the local coolant temperature. These two temperatures delimit the maximum temperature drop possible through the wall. The maximum achievable local heat flux is then set by the wall thickness (determined by structural loads and manufacturing constraints) and wall thermal conductivity. The local heat flux is maximum at the nozzle throat, its magnitude increasing with increasing chamber pressure or with decreasing effective throat diameter. At high chamber pressures and narrow throats, this is the limiting design constraint.

#### 2. *Heat Load Limit*

In a regeneratively cooled engine, propellants are used to cool the chamber and nozzle so that propellant temperature increases in the cooling channels. At a high enough total heat load, the propellant temperature approaches the wall temperature so that cooling ceases. For some propellants, thermal decomposition may also limit the maximum bulk coolant temperature. The total heat load limit is reached first at low chamber pressures, because the heat load is proportional to chamber pressure raised to a power of about 0.8 (from heat transfer correlations), whereas the heat capacity of the propellants scales with mass flow, that is, directly with pressure. This limitation is also encountered in engine configurations that have large ratios of internal surface area to throat area.

#### 3. *Residence Time Limit*

Complete combustion is required to realize all of the stored chemical energy of the propellants. The combustion process can be considered to consist of two sequential steps, propellant mixing followed by chemical reaction. The mixing time scales with chamber size, but the chemical reaction time is independent of chamber length scale (although it does depend on pressure and temperature). This implies that there is a minimum time that the propellants must spend in the chamber (about 100 $\mu$s) and, thus, a minimum required chamber volume. However, increasing chamber volume increases the internal surface area and, thus, the total heat load. Also, increased volume implies increased wafer area and/or increased fabrication complexity, both of which are expensive.

#### 4. *Turbine Power Limit*

In an expander cycle, the power required to drive the propellant pumps comes from the energy absorbed by the propellants as they cool the walls. This energy flux, equivalent to the total heat load, sets a maximum feasible pump exit pressure. For the range of pressures and engine sizes considered here, this does not appear to be an important constraint because the maximum heat flux constraint at the throat is typically encountered at a chamber pressure well below the pressure corresponding to the maximum feasible pump exit pressure.

### C. Fabrication Constraints

Whereas microrocket engines (and, in particular, the fine geometric features required) are enabled by the choice of silicon microfabrication technology, this technology also imposes constraints on the engine design. Specifically, the geometry must be created by removing material from a set of silicon wafers by a deep etching process. Wafers can be joined with diffusion bonding as long as the surfaces are smooth to a few nanometers. The specific etching technique used, deep reactive ion etching (DRIE), and the tools and process used in this work have been described and characterized by Ayon et al.[10,11] To first order, DRIE produces vertical walls that constrain the design to prismatic or extruded like features unlike those common to conventional rocket engines. As can be seen in Figs. 1 and 2, this results in a two-dimensional chamber and nozzle, rather than the more usual axisymmetric geometry. The etching technique also prefers that all of the features etched into one face of a wafer be

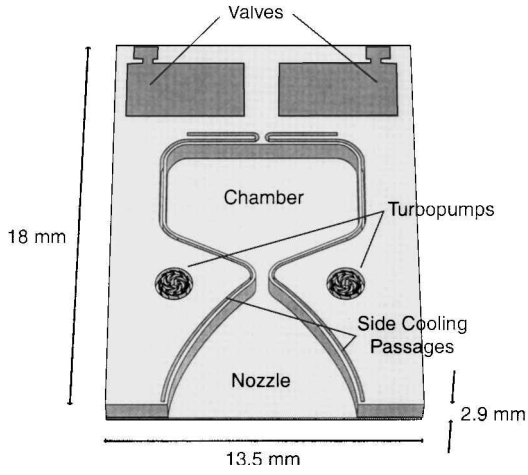


**Fig. 1 Conceptual layout of microrocket engine system.**

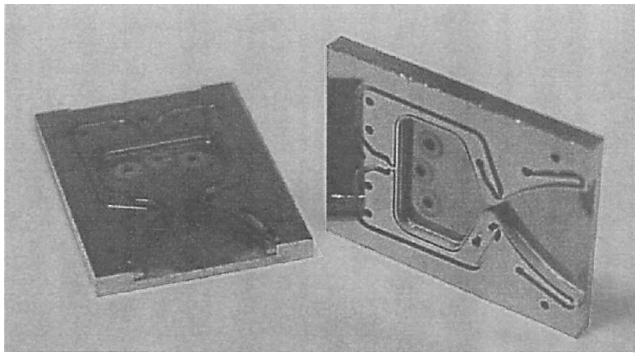

**Fig. 2 Two halves of microrocket thrust chamber and nozzle; nozzle exit is 7.5 mm wide.**

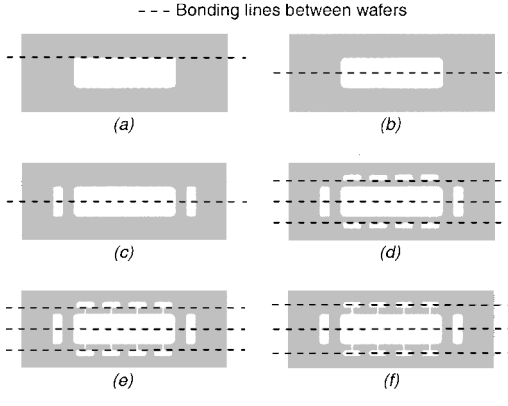


**Fig. 3 Potential wafer layouts for constructing microrocket (nominal cross-sectional views through chamber).**

of the same depth. The implications of these fabrication constraints on engine design are illustrated in the sequence of chamber cross sections in Fig. 3.

The simplest way to create the chamber and nozzle would be to etch the shape shown in Figs. 1 and 2 into a wafer and then cap it with another wafer, as shown in Fig. 3a. This presents a problem in that sharp corners (radii at the angstrom level) are formed at the wafer bond line. This would generate high stress concentrations when the chamber is pressurized. A better design is to etch half of the nozzle (with fillets at the bottom of the etch) into two identical wafers, which are then bonded as in Fig. 3b. Cooling passages around the chamber and nozzle are required for thermal integrity. Side cooling passages are readily added during the nozzle etch, as shown in Fig. 3c. However, cooling passages on the top and bottom surfaces of the chamber and nozzle require additional wafers. The two wafers defining the chamber and nozzle are thinned, and

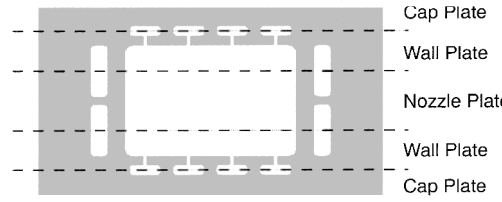


**Fig. 4 Additional wafers, termed nozzle plates, can be inserted along centerline to increase the height of the chamber and nozzle.**

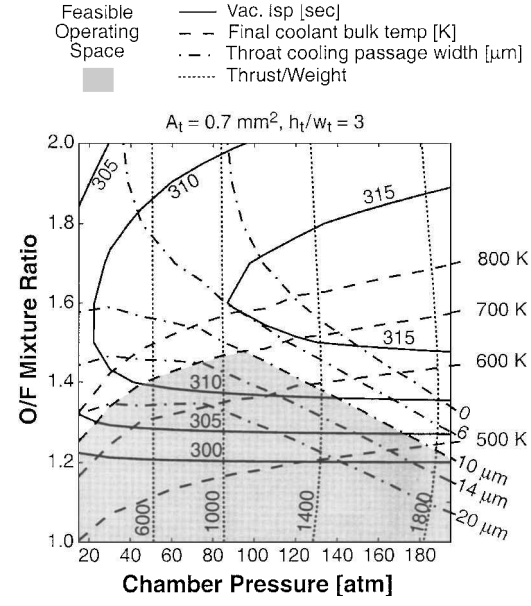


**Fig. 5 Feasible operating space of oxygen/ethanol microrocket engine.**

top and bottom cooling passages then etched into two additional wafers, as shown in Fig. 3d. This also allows propellant injectors, pressure taps, or igniter ports to be etched into the chamber wall on the opposite side of the wafers that contain the nozzle etch, as in Fig. 3e. However, this introduces the same problem as in Fig. 3a, that of sharp corners in locations of high stress, this time in the cooling channels. One solution is the nested masking fabrication technique that allows etches of different depths on the same side of the wafer. This enables the top and bottom cooling passages to span the bond line between the capping and nozzle wafers, as in Fig. 3f. This basic layout is suitable for an engine. If needed, one or more additional wafers can be inserted along the centerline, as in Fig. 4, to increase the chamber height. The baseline design incorporates two of these inserted nozzle plates.

### D. Feasible Design Space

The constraints just discussed define the feasible design space of a microrocket engine and, therefore, delimit the achievable performance as shown in Fig. 5 (see London[12] for details). This shows contour plots of $I_{sp}$ and thrust-to-weight ratio for an oxygen/ethanol engine over an operating space defined by chamber pressure and propellant mixture ratio. $I_{sp}$ is maximized at high chamber pressures and mixture ratios near 1.6. Thrust to weight increases nearly linearly with chamber pressure. The heat flux limitation is represented by the width of the cooling passage at the throat required to absorb this heat flux, and the total heat load is represented by the temperature to which the propellants are heated while cooling the chamber and nozzle walls. Current etching technique limits the feature size of deep trenches to no less than 10 $\mu$m. The maximum allowable wall temperature is 900 K, so that the maximum bulk final coolant temperature ($T_{bf}$) is approximately 700 K.

Only the shaded area of Fig. 5 meets all of the constraints. The upper boundary of this space defines the maximum specific impulse that can be achieved as a function of chamber pressure, termed

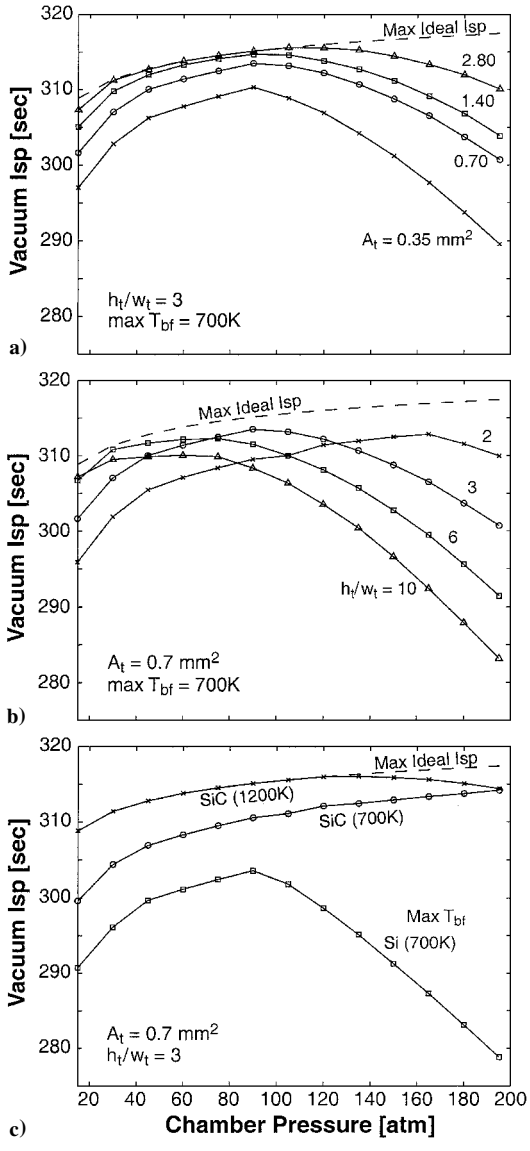


**Fig. 6 Dependence of the feasible $I_{sp}$ envelope on geometry and allowable wall temperature: a) $I_{sp}$ envelope expands with increasing throat area, b) peak of $I_{sp}$ envelope shifts to lower pressures as throat aspect ratio increases, and c) $I_{sp}$ envelope enlarges to near ideal level if silicon carbide is used for construction.**

the feasible $I_{sp}$ envelope. In this case, the achievable $I_{sp}$ is less than the ideal $I_{sp}$ at each chamber pressure, and there is a chamber pressure where the $I_{sp}$ is maximized. The operating space and, therefore, this $I_{sp}$ envelope, will depend on engine geometry, which can be characterized by the throat area $A_t$, a measure of the overall size of the engine, and the ratio of throat height to width ($h_t/w_t$), representing the shape of the engine. Figure 6a shows that the $I_{sp}$ envelope expands with increasing throat area, and Fig. 6b shows that the $I_{sp}$ envelope shifts toward lower pressures as the throat aspect ratio is increased. Finally, Fig. 6c shows the change in $I_{sp}$ envelope for a silicon carbide engine, which allows higher wall temperatures, shown as 1200 K in Fig. 6c.

These results show that $I_{sp}$ is maximized for large throat area, for example, large engine thrust, intermediate throat aspect ratio, and silicon carbide construction. However, additional factors influence design choices. First, the peak in the $I_{sp}$ envelope is broad, so that, for some applications, higher than ideal chamber pressures can increase the thrust-to-weight ratio at a modest penalty in $I_{sp}$. Second, fabrication difficulty is a major concern. There is relatively little experience in manufacturing such structures from silicon carbide, and so silicon is the initial material of choice. Third, increasing the throat area requires either more wafers (increasing fabrication complexity) or larger wafer area (yielding fewer engines per wafer set). A six-wafer baseline design was chosen that yielded 16 engines per wafer set, from 100-mm-diam wafers. The baseline design has a throat width of 0.5 mm, a throat height of 1.4 mm, a chamber pressure of 125 atm, and produces a nominal 15 N of thrust at an $I_{sp}$ of 300 s at an oxidizer-to-fuel ratio of 1.3. At a motor mass of 1.2 g, this would yield a thrust-to-weight ratio of greater than 1000:1.

## IV. Initial Demonstration

As an initial demonstration of this concept, a cooled thrust chamber has been designed, fabricated, and tested. A liquid-cooled, nonregenerative design was chosen for these proof-of-concept tests so that the liquid coolant flow could be set and monitored independently of the propellant flow to facilitate heat load measurement and reduce technical risk. Gaseous oxygen and methane were chosen as the propellants to minimize feed system complexity, and water or ethanol were used as coolants.

### A. Design and Fabrication

Though it uses different propellants, the thrust chamber was designed to match the size and thrust of the baseline oxygen and ethanol engine. A detailed thermal and structural design of the chamber was performed with two- and three-dimensional finite element analysis. As an example, the predicted temperature profile at a cross section through the throat is shown in Fig. 7. The cooling passages were

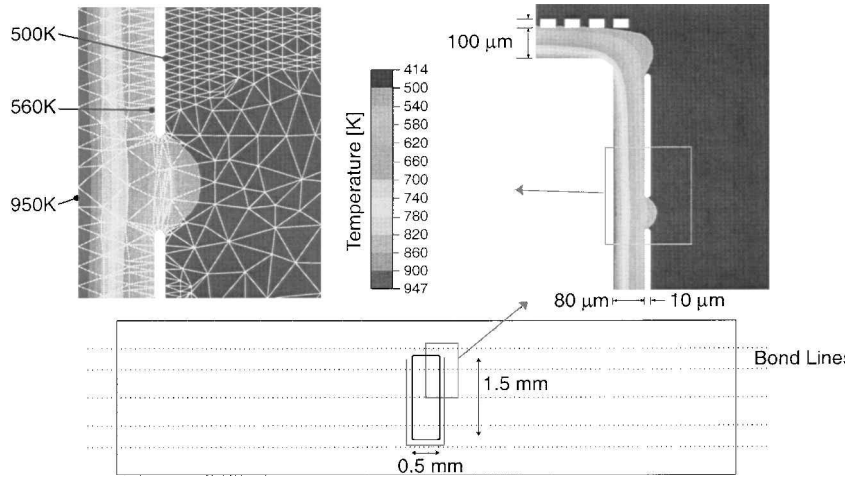


**Fig. 7 Calculated temperature profile through nozzle throat cross section.**

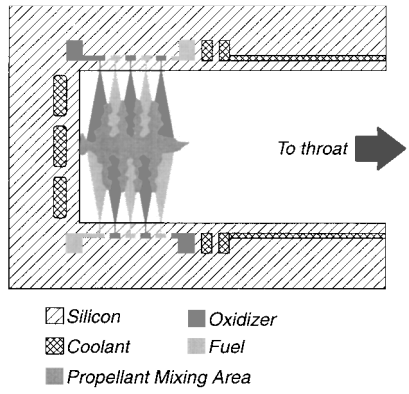


**Fig. 8 Cross section through chamber showing injection scheme concept.**

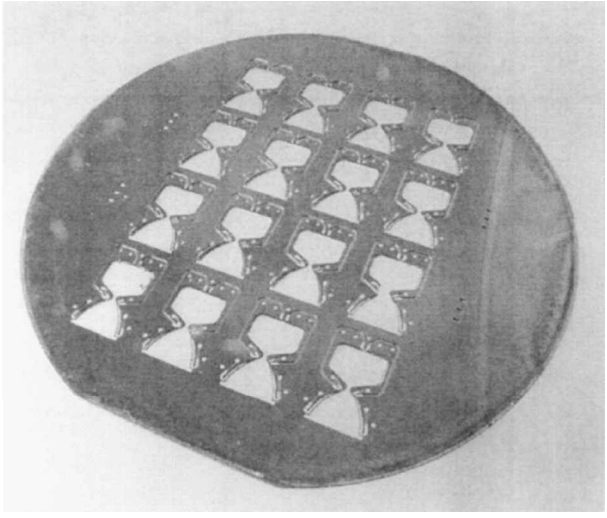

**Fig. 9 One of six 100-mm-diam wafers.**

sized to match the local heat flux predicted at each location. The coolant flow begins at the throat where the heat flux is largest, then cools the chamber, and finally is piped through the chip to cool the expansion nozzle.

At the current state of the art of microfabrication, it is very difficult to etch the injectors other than perpendicular to the flow direction, and so an unusual injection geometry was adopted. The fuel and oxidizer injectors are arranged in five rows at the rear of the chamber on the top and bottom walls in a checkerboard pattern. The pattern is reversed on top and bottom so that each oxidizer jet impinges on a fuel jet from the opposite wall, and vice versa. Figure 8 is a conceptual cross section through the chamber that illustrates this injection scheme. There are 484 injectors (242 for each propellant). The nominal injector diameter is 14 $\mu$m for the fuel and 18 $\mu$m for the oxidizer.

The final design is embodied in a set of nine masks that define the shapes to be etched into the six wafers during fabrication. The thrust chambers are manufactured from six silicon wafers, each about 0.5 mm thick. One wafer, 100 mm in diameter by 0.5 mm thick, is shown in Fig. 9. The six wafers are laminated together to form the 3-mm-thick, 18-mm-long, and 13.5-mm-wide thrust chamber, pictured in Fig. 2. The fabrication method is that of silicon bulk microfabrication. Essentially, this is a two-step process that is repeated on each side of each wafer. In the first step, a pattern is transferred to a masking material that has been precoated on a wafer. In the second step, this material then serves as a mask for the etching process, which removes material in the nonmasked areas, creating the necessary features of a given depth. Each side of the six wafers is etched separately, and then the six wafers are bonded together through an aligned fusion bonding process. Reference 12 describes

**Fig. 10 Thrust chamber and nozzle consists of six wafers.**

the fabrication and packaging of the thrust chamber in more detail. Figure 10 shows an exploded view of the six wafers that make up the thrust chamber stack. Figure 11 shows three cross sections of a fabricated thrust chamber, along with a line drawing overlay of all of the nine masks, illustrating the geometric features of the thrust chamber. An interior corner of the combustion chamber is shown in Fig. 12, showing the propellant injectors and cooling channels.

### B. Test Setup

An automated test stand was built to supply and meter propellants and coolant and to measure thrust, flow rates, temperatures, and pressures. The propellant and coolant supply system are designed for

delivery pressures up to 400 atm. Flow rates are measured with mass flow meters. Pressures are measured in the supply and exit lines and at the chip interface. These include propellant supply, coolant supply and exit, and chamber static. Temperature is measured with 25-$\mu$m-diam thermocouples on the chip and chip interface tubing and with an imaging infrared radiometer. Thrust is measured directly with a load cell. The overall accuracy of the measurements is indicated by error bars on the data to follow. Details of the test apparatus, its calibration, and error analysis may be found in Ref. 12.

A single spark in the combustion chamber ignites the engine. The test procedure was to start the motor at low chamber pressure, ramp up the flow rate, record data at steady state for 4 s, and then ramp up the flow rate again, etc.

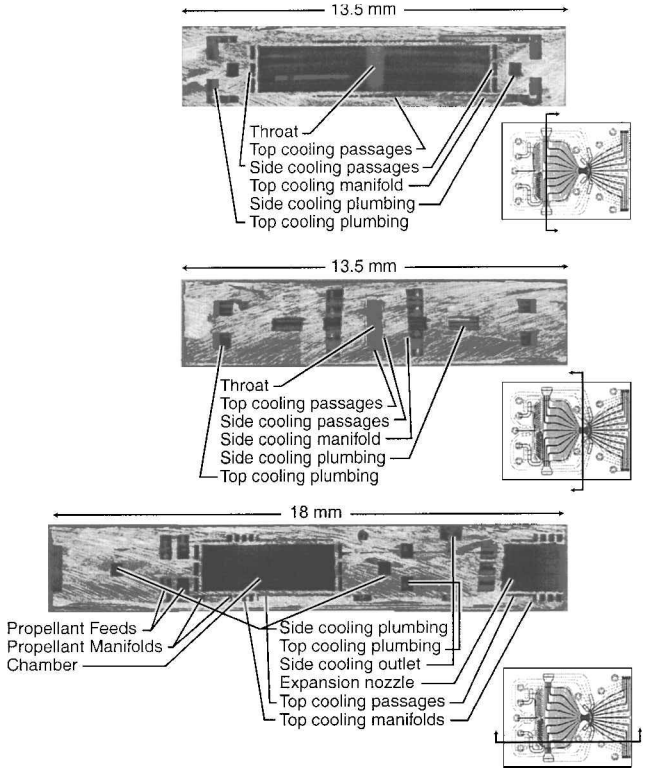


**Fig. 11 Cross sections of fabricated thrust chamber.**

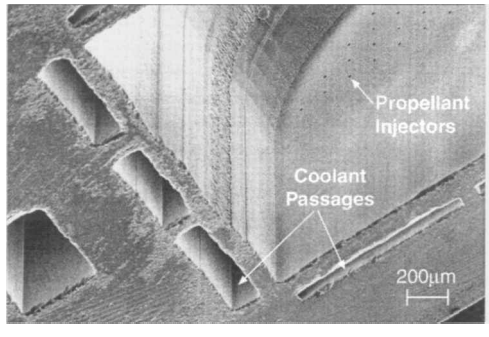


**Fig. 12 Motor cutaway showing cooling channels and propellant injectors.**

### C. Experimental Results and Analysis

Results are reported here for three motors, all using water as a coolant. Data from three steady-state conditions are considered: ignition at low chamber pressure (2 atm), an intermediate pressure (7 atm), and a higher pressure (12.3 atm). Figure 13 shows time traces of measured chamber pressure and thrust (the slower rise time of pressure reflects slower instrument response). The highest thrust shown is approximately 1 N at a chamber pressure of 12.3 atm. This corresponds to a motor thrust-to-weight ratio of 85:1. Engines survived cold pressure testing to pressures above 120 atm. In hot tests, however, the motors failed at chamber pressures above 12.3 atm, at a location immediately downstream of the injectors. Subsequent analysis suggests that cooling is inadequate in the area where the top and bottom cooling channels transition into collection headers. A revised cooling scheme will be tested in subsequent versions of the engine. Therefore, the data reported herein are restricted to pressures no higher than 12.3 atm.

Specific impulse ($I_{sp}$) is the most important measure of chemical rocket engine performance. $I_{sp}$ can be expressed in terms of a thrust coefficient $C_F$ and a characteristic exhaust velocity $c^*$ as follows:

$$I_{sp} = c/g = C_F c^* / g \tag{1}$$

Where $c^* = P_c A_t / \dot{m}$ and $C_F = F / P_c A_t$ where $P_c$ is chamber pressure, $A_t$ is the throat area, $F$ is the thrust, and $\dot{m}$ is the total propellant mass flow rate. The $c^*$ is a measure of the combustion completeness, and $C_F$ is a measure of the expansion nozzle performance. Each will be considered in turn hereafter.

#### 1. *Characteristic Exhaust Velocity*

The characteristic exhaust velocity $c^*$, inferred from the experimental measurements in three runs is shown as a function of chamber pressure in Fig. 14. In Fig. 14, three predicted values of $c^*$ are shown for each of the experimental points, evaluated at the respective experimental conditions. These predictions are performed using the NASA CEA code[13] and assume equilibrium chemistry. As the chamber pressure increases from about 2 to 7 atm, $c^*$ initially increases, but then remains essentially constant as the chamber pressure increases from 7 to 12 atm. Because chemical reaction rates typically scale with pressure to a power larger than one, this implies

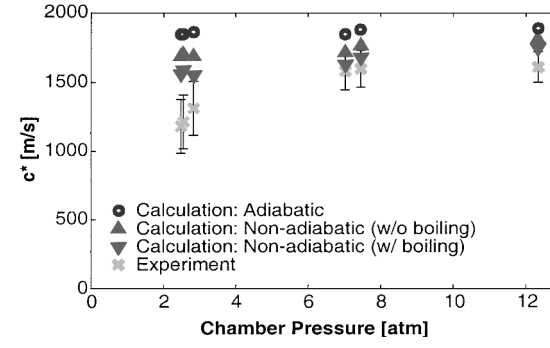


**Fig. 14 Experimental and calculated characteristic velocity $c^*$.**

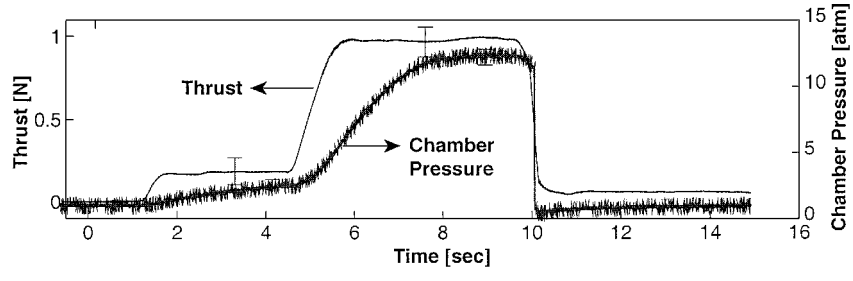


**Fig. 13 Time history of thrust and chamber pressure.**

that the kinetics of the reactions are not limiting the combustion process.

At the run conditions ($P_c = 7$ and 12 atm), the experimental $c^*$ appears to be approximately 15% below the expected adiabatic value. However, there is significant heat loss in the experiment, which can be quantified by measuring the enthalpy rise of the coolant. Reference 12 presents two ways of estimating this heat loss. The first is a conservative estimate that assumes no energy is stored in the phase change of the coolant, whereas the second estimate includes the effect of boiling some fraction of the coolant. When these heat losses are included, the predicted $c^*$ falls within the uncertainty bounds of the experimental values.

That the experimental values of $c^*$ agree well with equilibrium chemistry predictions implies that the residence time is sufficient for complete combustion, that is, the injection and mixing processes in the combustion chamber are complete. It also implies that, in a regenerative configuration, $c^*$ for the microrocket engine should be about the same as for a large motor.

*2. Thrust Coefficient*

The thrust coefficient calculated from the experimental data is shown in Fig. 15. The nozzle was designed with an expansion ratio of 15, based on a design chamber pressure of 125 atm and atmospheric exhaust. Because the maximum chamber pressure for these tests is only 12.3 atm, separation in the nozzle is to be expected and is observed in visual and infrared (3–5 $\mu$m) images as illustrated in Fig. 16. At the higher chamber pressure the plume is bifurcated, apparently an artifact of a high-aspect-ratio (5.4:1) rectangular nozzle operated far from design. The highly three-dimensional flow in this nozzle at the off-design experimental conditions is complex and unusual, and so, as a first approximation, an idealized one-dimensional relationship was used for $C_F$. The influence of flow separation is introduced through a parameter equal to the ratio of the pressure in the flow at separation $P_{sep}$ to the ambient pressure $P_{amb}$. For axisymmetric nozzles, the value of this ratio is typically 0.4 (Sutton[14]), which is shown as the upper theoretical curve in Fig. 15. Setting this ratio to 0.2 yields the lower curve in Fig. 15.

Though it is difficult to accurately predict nozzle performance given that an unusual nozzle geometry is operating far from design, the experimental results agree qualitatively with the range of expected values. This implies that viscous effects in the nozzle do not appreciably limit the system performance. A more meaningful assessment of nozzle performance limitations would require either operating the engine closer to the nozzle design point, or redesigning the nozzle for the lower operating pressure.

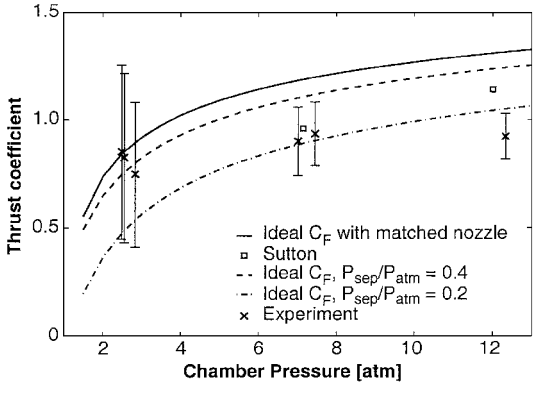


**Fig. 15 Experimental and idealized thrust coefficient $C_f$.**

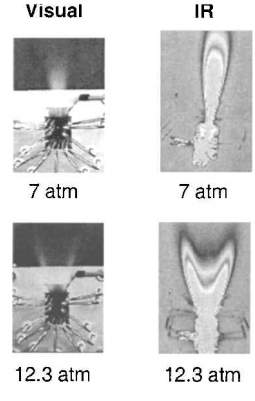


**Fig. 16 Visual and infrared images of motor and exhaust plume at two chamber pressures.**

*3. Specific Impulse*

The combined effect of $C_F$ and $c^*$ is the specific impulse $I_{sp}$. Although the measured value of approximately 150 s is low relative to that of typical $I_{sp}$ of large bipropellant engines operated near their design conditions (typically 300–350 s), it is consistent with a large engine operated off-design at sea level with a chamber pressure near 10 atm. Realizing higher $I_{sp}$ requires increasing $C_F$ because $c^*$ is near its ideal value. $C_F$ can be improved by increasing the chamber pressure to ambient pressure ratio or by redesigning the expansion nozzle for the current pressure ratio. If the present tests had been performed in vacuum, one would expect a $C_F$ near its limiting value of 1.8, corresponding to an $I_{sp}$ of 290–295 s. The results to date suggest that this level of specific impulse could also be achieved by increasing the chamber pressure to its design value of 125 atm. We are presently focused on the latter.

## V. Conclusions

The concept of a bipropellant rocket engine micromachined from silicon using semiconductor manufacturing technology has been introduced. A number of potential applications have been discussed, and the primary engineering requirements and constraints have been identified. To evaluate the feasibility of the concept, a thrust chamber has been designed, fabricated, and tested. The results to date are encouraging, with demonstrated thrusts of up to 1 N at chamber pressures of above 12 atm, corresponding to a thrust-to-weight ratio of 85:1. The measured characteristic exhaust velocity, a measure of combustion effectiveness, is within 5–10% of its ideal value, suggesting that combustion is complete. Work is ongoing to realize the design thrust of 15 N by redesign of the cooling jacket.

## Acknowledgments

This research was primarily sponsored by NASA John H. Glenn Research Center at Lewis Field, Steven Schneider, Technical Monitor. Additional support has been provided by the U.S. Army Research Office, T. Doligalski, technical manager; by the Defense Advanced Research Projects Agency, R. Rosenfeld, Program Manager; and by the Massachusetts Institute of Technology (MIT) Lincoln Laboratory Advanced Concepts Committee. The authors thank H. Feinstein of Lincoln Laboratory for the design of the engine test stand and C. Protz for Fig. 12. The authors would also like to acknowledge Arturo Ayon, Martin Schmidt, Yoav Peles, Kurt Broderick, and other members of the Microsystems Technology Laboratory at MIT for their advice and assistance in the microfabrication phase of this work.

## References

[1] Epstein, A. H., and Senturia, S. D., "Macro Power from Micro Machinery," *Science*, Vol. 276, No. 5316, 1997, p. 1211.

[2] Epstein, A. H., Senturia, S. D., Al-Midani, O., Anathasuresh, G., Ayon, A., Breuer, K., Chen, K.-S., Ehrich, F. F., Esteve, E., Frechette, L., Gauba, G., Ghodssi, R., Groshenry, C., Jacobson, S. A., Kerrebrock, J. L., Lang, J. H., Lin, C.-C., London, A., Lopata, J., Mehra, A., Mur Miranda, J. O., Nagle, S., Orr, D. J., Piekos, E., Schmidt, M. A., Shirley, G., Spearing, S. M., Tan, C. S., Tzeng, Y.-S., and Waitz, I. A., "Microheat Engines, Gas Turbines, and Rocket Engines: The Massachusetts Institute of Technology Microengine Project," AIAA Paper 97-1773, 1997.

[3] London, A. P., "A Systems Study of Propulsion Technologies for Orbit and Attitude Control of Microspacecraft," M.S. Thesis, Dept. of Aeronautics and Astronautics, Massachusetts Inst. of Technology, Cambridge, MA, June 1996.

[4] Al-Midani, O., "Preliminary Design of a Liquid Bipropellant Microfabricated Rocket Engine," M.S. Thesis, Dept. of Aeronautics and Astronautics, Massachusetts Inst. of Technology, Cambridge, MA, June 1998.

[5] Protz, C., "Systems Analysis of a Microfabricated Storable Bipropellant Rocket Engine," M.S. Thesis, Dept. of Aeronautics and Astronautics, Massachusetts Inst. of Technology, Cambridge, MA, Jan. 2000.

[6]Lopata, J., "Characterization of Heat Transfer Rates in Supercritical Ethanol for Micro-Rocket Engine Regenerative Cooling," M.S. Thesis, Dept. of Aeronautics and Astronautics, Massachusetts Inst. of Technology, Cambridge, MA, Sept. 1998.

[7]Faust, A., "Forced Convective Heat Transfer to Supercritical Water in Micro-Rocket Cooling Channels," M.S. Thesis, Dept. of Aeronautics and Astronautics, Massachusetts Inst. of Technology, Cambridge, MA, Feb. 2000.

[8]Frechette, L., "Development of a Microfabricated Silicon Motor-Driven Compressor System," Ph.D. Dissertation, Dept. of Aeronautics and Astronautics, Massachusetts Inst. of Technology, Cambridge, MA, Sept. 2000.

[9]Francis, R. A., "Systems Study of Very Small Launch Vehicles," M.S. Thesis, Dept. of Aeronautics and Astronautics, Massachusetts Inst. of Technology, Cambridge, MA, Sept. 1999.

[10]Ayon, A., Lin, C., Braff, R., Bayt, R., Sawin, H., and Schmidt, M., "Characterization of a Time Multiplexed Inductively Coupled Plasma Etcher," *Journal of the Electrochemical Society*, Vol. 146, No. 1, 1999, pp. 339–349.

[11]Ayon, A., Braff, R., Bayt, R., Sawin, H., and Schmidt, M., "Influence of Coil Power in the Etching Characteristics in a High Density Plasma Etcher," *Journal of the Electrochemical Society*, Vol. 146, No. 7, 1999, pp. 2730–2736.

[12]London, A. P., "Development and Test of a Microfabricated Bipropellant Rocket Engine," Ph.D. Dissertation, Dept. of Aeronautics and Astronautics, Massachusetts Inst. of Technology, Cambridge, MA, June 2000.

[13]Gordon, S., and MacBride, B., "Computer Program for Calculation of Complex Chemical Equilibrium Compositions and Applications," NASA RP-1311, 1994.

[14]Sutton, G. P., *Rocket Propulsion Elements*, 6th ed., John Wiley & Sons, New York, 1992, pp. 58–72.